Nanopatterning spin-textures: A route to reconfigurable magnonics

E. Albisetti, D. Petti, M. Madami, S. Tacchi, P. Vavassori, E. Riedo, and R. Bertacco

Citation: AIP Advances **7**, 055601 (2017); doi: 10.1063/1.4973387
View online: http://dx.doi.org/10.1063/1.4973387
View Table of Contents: http://aip.scitation.org/toc/adv/7/5
Published by the American Institute of Physics

Nanopatterning spin-textures: A route to reconfigurable magnonics

E. Albisetti,[1,2,a] D. Petti,[1] M. Madami,[3] S. Tacchi,[4] P. Vavassori,[5,6] E. Riedo,[2,7] and R. Bertacco[1,8]

[1]*Dipartimento di Fisica, Politecnico di Milano, 20133 Milano, Italy*
[2]*CUNY-Advanced Science Research Center, New York, New York 10031, USA*
[3]*Dipartimento di Fisica e Geologia, Università di Perugia, Italy*
[4]*Istituto Officina dei Materiali del CNR (CNR-IOM), Unità di Perugia, c/o Dipartimento di Fisica e Geologia, Perugia, Italy*
[5]*CIC nanoGUNE, E-20018 Donostia,-San Sebastian, Spain*
[6]*IKERBASQUE, Basque Foundation for Science, 48013, Bilbao, Spain*
[7]*Department of Physics, CUNY-City College of New York, New York, New York 10031, USA and Physics Program, CUNY-The Graduate Center, New York, New York 10016, USA*
[8]*IFN-CNR, c/o Politecnico di Milano, 20133 Milano, Italy*

(Presented 3 November 2016; received 9 September 2016; accepted 8 October 2016; published online 23 December 2016)

Magnonics is envisioned to enable highly efficient data transport and processing, by exploiting propagating perturbations in the spin-texture of magnetic materials. Despite the demonstrations of a plethora of proof-of-principle devices, the efficient excitation, transport and manipulation of spin-waves at the nanoscale is still an open challenge. Recently, we demonstrated that the spin-wave excitation and propagation can be controlled by nanopatterning reconfigurable spin-textures in a continuous exchange biased ferromagnetic film. Here, we show that by patterning 90° stripe-shaped magnetic domains, we spatially modulate the spin-wave excitation in a continuous film, and that by applying an external magnetic field we can reversibly "switch-off" the spin-wave excitation. This opens the way to the use of nanopatterned spin-textures, such as domains and domain walls, for exciting and manipulating magnons in reconfigurable nanocircuits. [http://dx.doi.org/10.1063/1.4973387]

I. INTRODUCTION

The control of spin-waves in ferromagnetic materials holds the promise to enable energy-efficient information transport and wave-based computing, by exploiting the absence of Joule-losses, the vectorial nature and non-linearity of magnons.[1–4] Conventionally, the engineering of spin-waves is achieved via physically patterning magnetic nanostructures such as magnonic crystals and magnetic micro-nanowires.[5] The control of spin-waves in such structures led to the pioneering demonstrations of the basic building blocks of computing, such as logic-gates[6–8] and transistors,[9] however, fundamental limitations are still to be overcome before magnonics becomes appealing as a viable route beyond CMOS electronics. One of the most critical issues, in this sense, is the efficient excitation and control of spin-waves at the nanoscale. As a matter of fact, channeling and steering of spin-waves in patterned nanowires is highly inefficient, due to the need of an external magnetic field[10,11] for spatially shaping the magnetization profile. Recently, two different approaches were proposed as a solution, for overcoming the need of external fields. The first is based on a physically patterned nanomagnetic device which allows to locally manipulate and transmit spin-waves.[12] The second one, demonstrated by the authors of this paper, is based on nanopatterning the spin-texture of a

[a]Author to whom correspondence should be addressed. Electronic mail: edoardo.albisetti@polimi.it.

continuous film, stabilizing desired magnetic domain and domain wall structures at remanence.[13,14] In particular, we showed the spatially controlled spin-wave excitation and propagation in magnetic domains patterned in a continuous exchange biased film via Thermally-Assisted Scanning Probe Lithography (*tam*-SPL). The absence of a physical patterning, the stability of exchange bias, and the full reversibility of the patterning allows for the vectorial writing of fully reconfigurable magnonic nanostructures.

In this work, we patterned 90° magnetic domains via *tam*-SPL in a continuous CoFeB/IrMn exchange bias bilayer. We show, via magnetic force microscopy and micromagnetic simulations, that sharp 90° domain walls are created at the boundaries of the patterned areas. Coplanar waveguides for exciting spin-waves in the CoFeB film were nanofabricated in correspondence of the *tam*-SPL patterns via Electron Beam Lithography (EBL). Micro-focused Brillouin Light Scattering (Micro-BLS) experiments were performed for mapping the spin-wave excitation intensity within and outside the patterns. We show the spatial modulation of the spin-wave excitation efficiency inside and outside the patterns at remanence. In addition, we show that, by applying an external bias field, the spin-wave excitation within the pattern can be reversibly suppressed.

These results, together with the recent demonstration of the use of domain walls as spin-wave waveguides[15,16] and short-wavelength spin-wave emitters,[17,18] lay the path to the integration of complex functionalities in fully reconfigurable nanoscale magnonic devices.

II. EXPERIMENTAL

Tam-SPL patterning was performed on a CoFeB 5/IrMn 7/Ru 2 (thickness in nm) magnetic multilayer grown by DC magnetron sputtering on a Si/SiO_2 substrate, with a base pressure below 1 x 10^{-8} Torr, in an AJA ATC Orion8 system. The CoFeB/IrMn bilayer constitutes the exchange bias system, and the top Ru layer is used as a capping layer. In order to tailor the blocking temperature (T_B) of the exchange bias system, a controlled 18.5% concentration of Ru impurities was included in the IrMn antiferromagnetic layer, as explained in Ref. 19. During deposition, a 300 Oe magnetic field H_g was applied in the sample plane for setting the uniaxial magnetic anisotropy direction in the CoFeB layer, and for setting the direction of the exchange bias in the as-grown sample. 60 x 60 μm^2 numbered squares were patterned via optical lithography and lift-off, in order to facilitate the location of the *tam*-SPL patterns and the alignment in the subsequent lithographic steps. After deposition, the sample underwent a thermal annealing at 200° C for 5'. Subsequently, it underwent a magnetic field cooling in a H_i = 4000 Oe field (initialization field) down to room temperature for setting a uniform exchange bias in the sample. H_i was set in the same direction as H_g. Magnetic characterization of the sample was performed at room temperature via Vibrating Sample Magnetometry (VSM) in a Microsense system.

During *tam*-SPL patterning, the heateable AFM tip heats the underlying region above the blocking temperature of the system. When the tip is displaced, the previously heated region undergoes a local field-cooling which re-sets the exchange bias in the direction of the CoFeB magnetization, set by the external magnetic field H_w.[13] *Tam*-SPL was performed in a customized Keysight 5600LS scanning probe system, equipped with silicon cantilevers integrated with a Joule resistive heater.[20,21] A National Instruments DAQ NI USB-6211 in combination with MATLAB scripts and Keysight PicoView software were employed for controlling the heater temperature and the tip movement. For patterning, the thermal cantilever was raster-scanned in a zig-zag fashion in contact mode with a speed of 3 $\mu m\ s^{-1}$. The separation between the lines during the scan was set to 62.5 nm. The measured Joule power dissipated by the tip resistive heater was around 35 mW. A magnetic sample holder was used to generate a uniform H_w = 700 Oe external magnetic field in the sample plane during patterning. Magnetic Force Microscopy (MFM) was performed with the same Keysight 5600LS system, upon replacing the heatable AFM tip with a magnetic one, in lift mode with a 100 nm lift height.

After *tam*-SPL patterning, a 30 nm thick SiO_2 layer was deposited via RF magnetron sputtering for insulating purposes. Nanofabrication of the coplanar waveguides (CPW) was performed via Electron Beam Lithography (EBL) using a LEO system equipped with Elphy Plus Raith pattern generator. The Ti 7/Au 100 bilayer was deposited by DC magnetron sputtering.

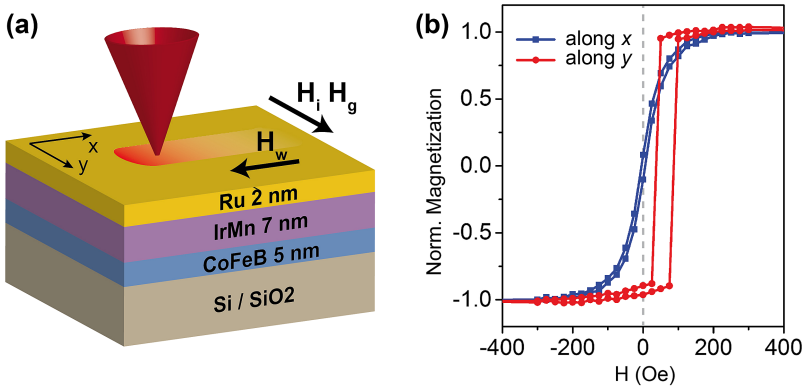

FIG. 1. (a) Sketch of the CoFeB/IrMn/Ru exchange bias multilayer used for patterning. The black arrows indicate the direction of the external magnetic field applied during the initial field cooling (H_i, along $+y$), and during patterning (H_w, along $-x$). (b) Magnetic characterization of the multilayer performed via vibrating sample magnetometry (VSM) on the sample after the initial field cooling. The easy-axis hysteresis loops (red line and circles) presents an exchange bias around 60 Oe. The blue line and squares shows the hard-axis loop.

Simulations of the micromagnetic configuration at remanence were performed using Object Oriented MicroMagnetic Framework (OOMMF) platform.[22] The exchange bias was modeled as a fixed external field acting on the 5 nm thick CoFeB layer, with intensity 60 Oe (according to the experimental hysteresis loops, see Fig. 1(b)) and directed along $-x$ and $+y$ inside and outside the patters, respectively. The parameters used include: CoFeB cell with size 10 nm x 10 nm x 5 nm, saturation magnetization $M_s = 1140$ kA/m, magneto-crystalline anisotropy 10^3 J/m^3 along y, damping coefficient $\alpha = 0.5$ and exchange stiffness $A_{ex} = 1.2 \times 10^{-11}$ J/m.[23,24]

Micro-BLS experiments were performed employing a 5 mW power monochromatic light at 532 nm wavelength from a diode-pumped solid-state laser. The light was focused on the sample using a microscope dark-field objective of NA = 0.75 and a super-long working distance of 4.7 mm.[25] In order to visualize the laser spot and the sample surface, a coaxial viewing system based on using the same objective and a collimated LED source at 455 nm was employed. For exciting spin-waves, a microwave current was injected in the ground-signal-ground coplanar waveguides using a picoprobe. During μ−BLS measurements, the sample holder and BLS spectrometer were controlled by TFPDAS4-MICRO and TFPDAS4 software, developed at Kaiserslautern University, which provided active stabilization of the lateral and vertical positions of the sample with a precision of ~50 nm.

III. RESULTS AND DISCUSSION

A sketch of the CoFeB/IrMn/Ru microfabricated magnetic multilayer is shown in Fig. 1(a). H_g indicates the direction of the magnetic field applied during the growth for setting the uniaxial anisotropy and exchange bias in the as-deposited sample. H_i marks the direction of the field applied during the initial field cooling, used for setting a uniform exchange bias in the whole sample. H_w, the writing field, is applied during *tam*-SPL at 90° with respect to H_i and determines the exchange bias direction within the patterned regions, and therefore the direction of the magnetization at remanence. In Fig. 1(b), the VSM hysteresis loops of the CoFeB layer after the initial field cooling are shown. In the graph, the red line with circles corresponds the easy-axis loop measured along the exchange bias direction (y direction). The loop is shifted from zero of a quantity $H_{eb} = 60$ Oe by the exchange interaction with IrMn. The blue line with squares represents the un-shifted hard-axis loop measured in the perpendicular direction (along x).

Fig. 2 shows the magnetic characterization and micromagnetic simulations of the magnetic structures patterned on the CoFeB/IrMn/Ru sample of Fig. 1 via *tam*-SPL, as explained in the experimental section. As shown in the MFM image of panel (a), acquired at remanence, the structures consist of two 29 μm x 2.5 μm stripes separated by 2.4 μm. In the MFM image, the direction of the magnetization within and outside the pattern is indicated in white. In particular, within the patterns the

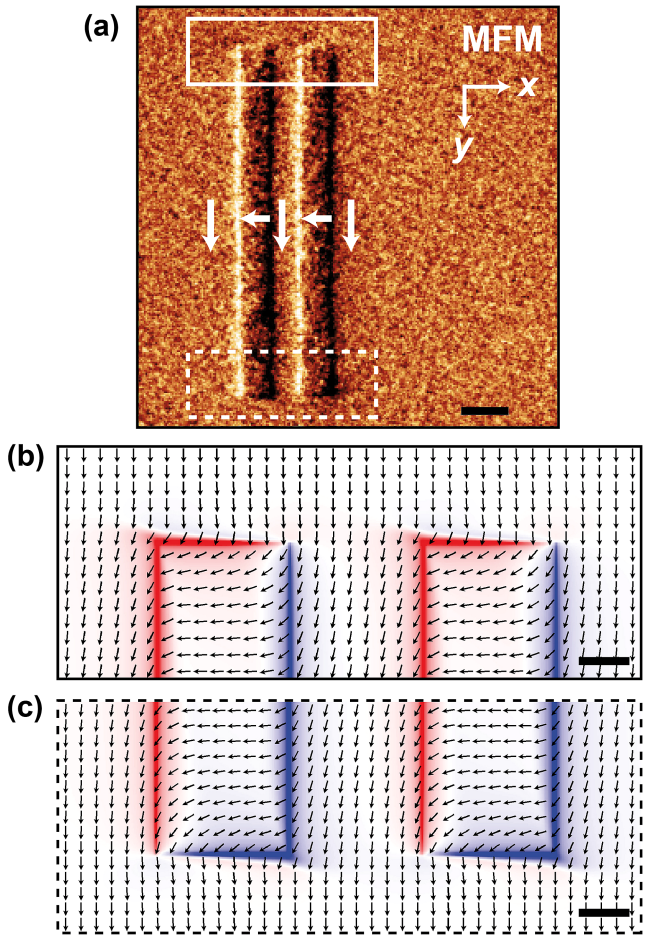

FIG. 2. (a) MFM image of the magnonic structures, consisting of two rectangular tracks, spaced by 2.4 μm. The static magnetization (white arrows) within the pattern forms a 90 degrees angle with respect to the magnetization outside. Scale bar: 4 μm. (b), (c) Micromagnetic simulations of the spin configuration in the top part (white solid square in panel (a)) and bottom part (white dashed square in panel (a)) of the pattern, respectively. The black arrows indicate the local magnetization direction; the red/blue colors mark the presence of magnetic charges due to the non-uniform magnetization. Scale bar: 1 μm.

magnetization lies along $-x$, while outside the patterns it is uniformly directed along $+y$. The stray magnetic field arising from the sharp 90° domain walls at the boundaries of the patterned regions gives rise to the bright/dark contrast observed in the MFM image. In panel (b) and (c), the OOMMF micromagnetic simulations of the top and bottom part of the patterns, respectively, are shown. The black arrows indicate the local direction of the magnetization, while the red/blue colors represent the divergence of the magnetization, indicating the presence of opposite magnetic charges, which can be qualitatively related to the opposite contrast observed in the MFM image in panel (a).[26] The simulations, in good accordance with the MFM image, show 90° domain walls at the boundaries of the stripes, while inside the pattern the magnetization is uniformly oriented along $-x$.

Coplanar waveguides, oriented perpendicularly to the long edge of the rectangular patterns, i.e. along x, with ground-to-ground distance of 5.5 μm were fabricated by EBL and lift-off as explained in the experimental section. Fig. 3 shows the optical image of the sample after the microfabrication process. The *tam*-SPL patterns are sketched as orange rectangles. H_{rf} indicates the direction of the microwave magnetic field generated by the CPW, while H_{ext} refers to the direction of the external magnetic field applied during the μ−BLS measurements. Referring to the MFM image of Fig. 2(a), it is worth noting that, inside the patterns, the static magnetization is parallel to the CPW arms, along -x, whereas, in the rest of the pad, the magnetization is perpendicular to the CPW, i.e. along $+y$.

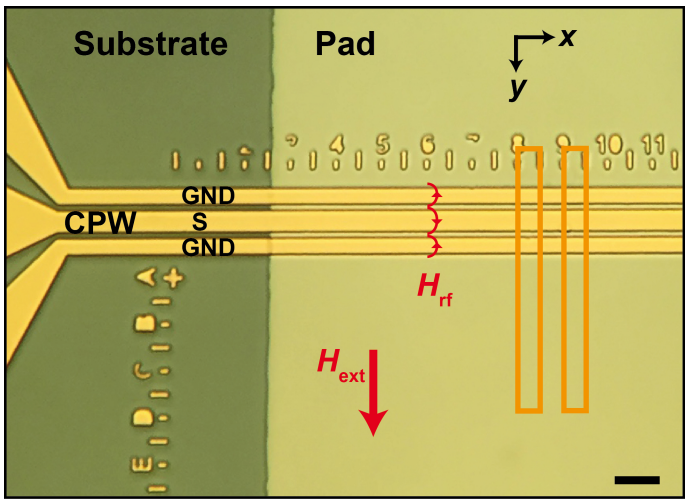

FIG. 3. Optical image of the sample, showing the coplanar waveguides (CPW) generating the Oersted field H_{rf} and the pad where the tam-SPL patterning was performed. The orange rectangles mark the position and shape of the structures shown in Fig 2. The red arrow marks the direction of the external magnetic field H_{ext} applied during the micro-BLS measurements. Scale bar: 5 μm.

Micro-BLS measurements were taken in order to map the spin-waves excitation intensity inside and outside the patterned tracks, when a microwave current was injected in the CPW. Fig. 4(a) shows the color-coded SWs intensity in the frequency range from 2.7 GHz to 8.3 GHz, as a function of the x-position. The BLS linear scan was performed in the region between the signal (S) and the ground (GND) lines of the CPW in order to maximize the SWs signal intensity thus reducing the acquisition time. The orange dashed lines indicate the boundaries of the patterned regions, and the white arrows indicate the static magnetization direction. The top panel of Fig 4(a) shows the spin-waves intensity map measured at remanence. It is worth noting that, in this configuration, spin-waves are efficiently excited within the patterns, i.e. 2.4 μm $< x <$ 4 μm and 7.5 μm $< x <$ 9 μm, while the spin-waves excitation efficiency is significantly lower in the rest of the pad. In Fig. 4(b) the Micro-BLS spectra acquired inside the pattern, at x = 3 μm, red star in panel (a), and outside the pattern, at x = 6 μm, blue star in panel (a), are compared quantitatively, showing that the spin-wave intensity measured inside the tracks (red squares) is about five time more intense than that measured outside (blue circles). This behavior can be explained taking into account the parallel (perpendicular) orientation of the in-plane component of the microwave field, produced by the CPW, with respect to the in-plane component of the dynamical magnetization within (outside) the tracks, as explained in detail in Ref. 13.

In the bottom panel of Fig. 4(a), we show that it is possible to reversibly "switch-off" the spin-wave excitation within the pattern by reorienting the magnetization with an external magnetic field. Fig. 4(a) (bottom panel) presents the intensity map acquired while applying a magnetic field H_{ext} = 300 Oe along the y-axis. As shown in Fig. 1(b), this intensity of the external field is high enough to fully rotate the magnetization of our exchange bias system along +y. In this configuration, the static magnetization is aligned perpendicularly to the CPW, both inside and outside the tracks and, as a consequence, the same low spin-wave intensity is observed in the whole pad. This is confirmed by the quantitative comparison of the BLS spectra shown in Fig. 4(c). Note also, that the SWs frequency inside the tracks is about 0.5 GHz lower than in the rest of the pad, in agreement with the different local effective field arising from the different orientation of the exchange bias field set inside and outside the tracks, with respect to the external applied field H_{ext}. It is worth noting, that the initial configuration shown in Fig. 4(a) is completely restored by the exchange bias field upon removal of the external field. As demonstrated in Ref. 13, the patterning is reconfigurable, and it can be erased and rewritten with a combination of heating and external field. In this paper, we demonstrate that this "hardware-reconfigurability" is combined with the active tuning of the pattern and its magnonic response via external magnetic fields.

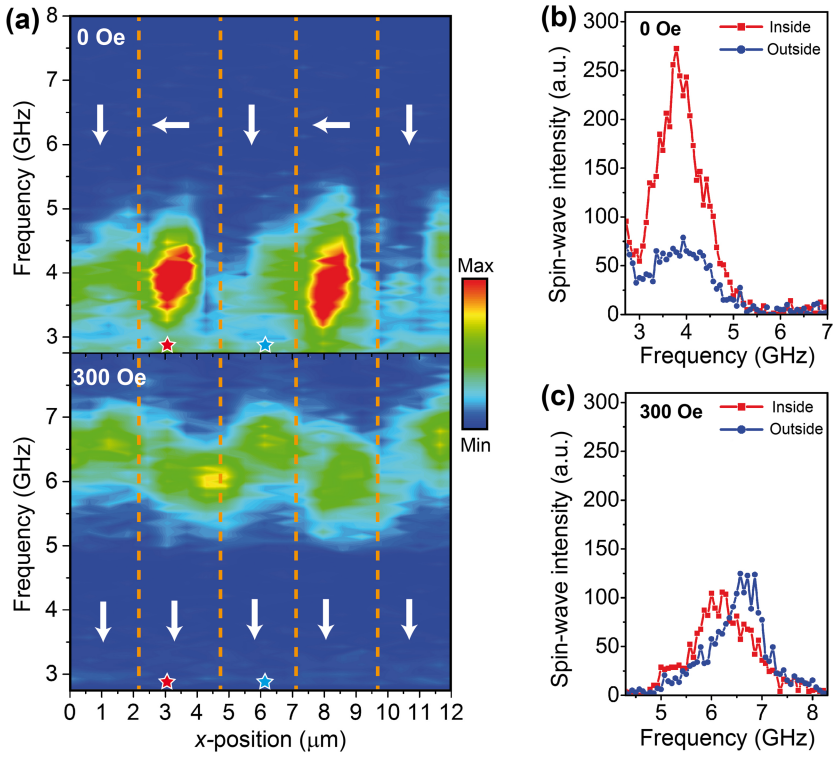

FIG. 4. (a) One-dimensional mapping of the spin-wave intensity measured by micro-BLS along the *x*-direction, between the signal (S) and the ground (GND) of the CPW. At remanence (top panel), spin-waves are efficiently excited exclusively within the patterned tracks, where the static magnetization lies parallel with respect to the CPW. By applying a magnetic field H_{ext} = 300 Oe as shown in Fig. 3, the spin-wave excitation within the tracks is 'switched-off' (bottom panel). (b), (c) Spin-wave spectra extracted respectively from the top and bottom panel of (a), inside (red squares) and outside (blue circles) the tracks. The spectra are related to the positions marked by the stars in panel (a).

IV. CONCLUSION

In this work we show that it is possible to spatially modulate the spin-wave excitation in a continuous magnetic film by nanopatterning reconfigurable spin-textures via *tam*-SPL. Furthermore, the spin-wave excitation can be reversibly switched-off by applying an external magnetic field. The ability to control the spin-wave excitation, propagation and interaction at remanence by patterning spin-textures, and the possibility to reversibly modulate the magnonic response with external fields opens incredibly rich scenarios. In this framework, the implementation of novel ways for tailoring nanoscale magnetism, together with the search for optimized magnonic materials are core tasks for going beyond proof-of-concept experiments.

ACKNOWLEDGMENTS

The research leading to these results has received funding from the European Union's Horizon 2020 Programme through project SWING (grant agreement no. 705326). D.P. acknowledges support from Cariplo project UMANA (project no. 2013-0735). R.B. acknowledges support from Cariplo project MAGISTER (project no. 2013-0726). E.R. thanks the support of the Office of Basic Energy Sciences of the Department of Energy (DE 0000224414). P.V. acknowledges support from Basque Government (Project no. PI2015_1_19) and Spanish Ministry of Economy and Competitiveness [Project no. FIS2015-64519-R (MINECO/FEDER)]. This work was partially performed at Polifab, the micro- and nanofabrication facility of Politecnico di Milano.

[1] A. V. Chumak, V.I. Vasyuchka, A.A. Serga, and B. Hillebrands, Nat. Phys. **11**, 453 (2015).
[2] S. Neusser and D. Grundler, Adv. Mater. **21**, 2927 (2009).
[3] D. Grundler, Nat. Phys. **11**, 438 (2015).

[4] G. Csaba, A. Papp, and W. Porod, J. Appl. Phys. **115**, 17C741 (2014).
[5] M. Krawczyk and D. Grundler, J. Phys. Condens. Matter **26**, 123202 (2014).
[6] M.P. Kostylev, A.A. Serga, T. Schneider, B. Leven, and B. Hillebrands, Appl. Phys. Lett. **87**, 1 (2005).
[7] T. Schneider, A.A. Serga, B. Leven, B. Hillebrands, R.L. Stamps, and M.P. Kostylev, Appl. Phys. Lett. **92**, 022505 (2008).
[8] K.-S. Lee and S.-K. Kim, J. Appl. Phys. **104**, 053909 (2008).
[9] A. V. Chumak, A. A. Serga, and B. Hillebrands, Nat. Commun. **5**, 4700 (2014).
[10] S. Urazhdin, V.E. Demidov, H. Ulrichs, T. Kendziorczyk, T. Kuhn, J. Leuthold, G. Wilde, and S.O. Demokritov, Nat. Nanotechnol. **9**, 509 (2014).
[11] K. Vogt, F.Y. Fradin, J.E. Pearson, T. Sebastian, S.D. Bader, B. Hillebrands, A. Hoffmann, and H. Schultheiss, Nat. Commun. **5**, 1 (2014).
[12] A. Haldar, D. Kumar, and A.O. Adeyeye, Nat. Nanotechnol. **11**, 437 (2016).
[13] E. Albisetti, D. Petti, M. Pancaldi, M. Madami, S. Tacchi, J. Curtis, W.P. King, A. Papp, G. Csaba, W. Porod, P. Vavassori, E. Riedo, and R. Bertacco, Nat. Nanotechnol. **11**, 545 (2016).
[14] E. Albisetti and D. Petti, J. Magn. Magn. Mater. **400**, 230 (2016).
[15] F. Garcia-Sanchez, P. Borys, R. Soucaille, J.-P. Adam, R.L. Stamps, and J.-V. Kim, Phys. Rev. Lett. **114**, 247206 (2015).
[16] K. Wagner, A. Kákay, K. Schultheiss, A. Henschke, T. Sebastian, and H. Schultheiss, Nat. Nanotechnol. **11**, 432 (2016).
[17] S.J. Hermsdoerfer, H. Schultheiss, C. Rausch, S. Schaäfer, B. Leven, S.-K. Kim, and B. Hillebrands, Appl. Phys. Lett. **94**, 223510 (2009).
[18] B. Van de Wiele, S.J. Hämäläinen, P. Baláž, F. Montoncello, and S. van Dijken, Sci. Rep. **6**, 21330 (2016).
[19] P. Sharma, E. Albisetti, M. Monticelli, R. Bertacco, and D. Petti, Sensors **16**, 1030 (2016).
[20] R. Garcia, A.W. Knoll, and E. Riedo, Nat. Nanotechnol. **9**, 577 (2014).
[21] W.P. King, B. Bhatia, J.R. Felts, H.J. Kim, and B. Kwon, Annu. Rev. Heat Transf. **16**, 287 (2013).
[22] M.J. Donahue and D.G. Porter, 1999 OOMMF User's Guide, Version 1.0. Interagency Report NISTIR 6376 (2004).
[23] J. Cho, J. Jung, K.-E. Kim, S.-I. Kim, S.-Y. Park, M.-H. Jung, and C.-Y. You, J. Magn. Magn. Mater. **339**, 36 (2013).
[24] B. Cui, C. Song, Y.Y. Wang, W.S. Yan, F. Zeng, and F. Pan, J. Phys. Condens. Matter **25**, 106003 (2013).
[25] M. Madami, G. Gubbiotti, S. Tacchi, and G. Carlotti, Solid State Phys. **63**, 79 (2012).
[26] M.H. Park, Y.K. Hong, B.C. Choi, M.J. Donahue, H. Han, and S.H. Gee, Phys. Rev. B **73**, 094424 (2006).